Electronic Supplementary Material (ESI) for ChemComm.
This journal is © The Royal Society of Chemistry 2020

# Supporting Information

**Spatially Localized Electrodeposition of Multiple Metals via Light-Activated Electrochemistry for Surface Enhanced Raman Spectroscopy Applications**

*Rafael N. P. Colombo, Vinicius R. Gonçales*, Shreedhar Gautam, Richard Tilley, J. Justin Gooding*, Susana I. C. de Torresi **

## Experimental Methods

Silicon wafers (Siltronix, France) of two types were used:

i) Herein named "*crystalline Si*" consists of a Si(100) orientation, single-side polished, 500-550 $\mu m$ thick and resistivity of $10 - 20\ \Omega \cdot sq$

ii) Herein named "*amorphous Si*" consists of a heterojunction based on Si(100) orientation, single-side polished, 500-550 $\mu m$ thick and resistivity $< 0.003\ \Omega \cdot sq$, coated with a 1 $\mu m$ thick layer of intrinsic amorphous Si via plasma-enhanced chemical vapour deposition (PECVD).

Silicon pieces were modified as described previously;[1] Briefly, silicon platforms were immersed in hot piranha solution (**manage with caution**) for surface organic impurities removal, transferred to 2.5% HF (**manage with caution**) for 90 seconds for oxide-removal and immediately moved to distilled 1,8-nonadiyne under inert ultrapure argon atmosphere. All glassware was submitted to flame drying and 1,8-nonadiyne was degassed by freeze-thaw cycling. A Schlenk line was used to keep entire reactional environment under positive argon pressure and as free of oxygen and water. The resulting densely packed monolayer was previously shown to be efficient on preventing $SiO_x$ formation. **Figure S1** presents a scheme for clarity purposes.

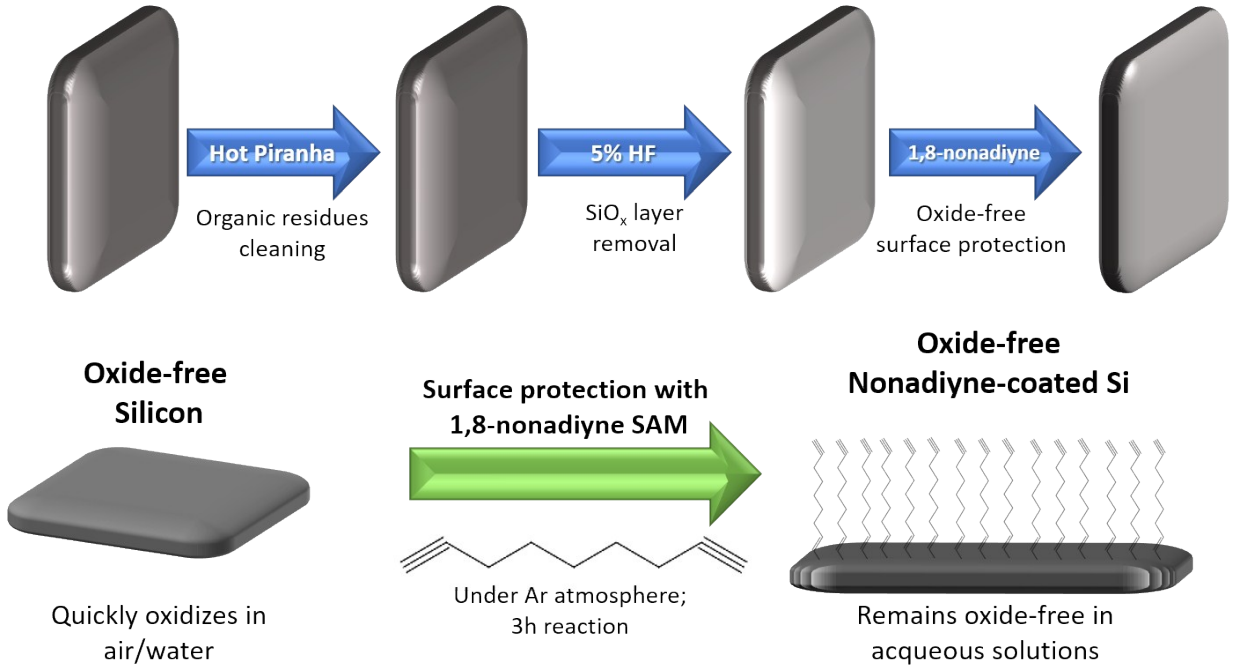


**Figure S1.** Representative scheme of silicon electrodes preparation. Pieces of approx. 1 cm x 1 cm were cut, immersed in hot piranha for cleaning, followed by immersion in 2.5% HF for removal of the silicon oxide layer that naturally forms in air and it was immediately transferred to a Schlenk flask with distilled and degassed 1,8-nonadiyne under ultrapure argon atmosphere. A densely packed layer is formed onto the surface and protects it against oxide formation; thus, the electrodes can be used for electrochemistry in aqueous solutions without typical impairment of oxide layer growth.

Plating baths were composed of freshly prepared (i) $HAuCl_4$ 10 mM + $K_2CO_3$ 250 mM; (ii) $AgNO_3$ 20 mM + $KNO_3$ 250 mM; (iii) $CuSO_4$ 50 mM + $K_2SO_4$ 250 mM.

During Au and Cu deposition an $Ag/AgCl/Cl^-_{3M}$ reference electrode was employed. For Ag deposition a clean silver wire was used as pseudo-reference to avoid chemical precipitation of AgCl at the reference junction and contamination of Si surface by AgCl.

All LAE depositions were performed potentiostatically with charge density cutoff values of 75 mC/cm² for Au and Cu and 50 mC/cm² for Ag. Between different plating steps, the electrochemical cell was thoroughly rinsed with deionized water. A CHI660D potentiostat was employed for electrochemical control. The custom-built light projector was controlled by MetroCon v3 software. LED source of 625 nm wavelength was used.

All SEM micrographs were acquired with a FEI NanoSEM 450 equipment; absence of silicon oxides was checked with XPS (ESCALAB, 220 iXL, Al Kα 1487 eV source).

Raman measurements were obtained with a Renishaw inVia equipment coupled to an optical microscope with 532 nm diode and 632.8 nm He/Ne lasers.

For Raman measurements, Si surfaces after electrodeposition of metallic particles were immersed in acetic acid for 10 seconds in order to remove eventual metal oxides and blown dry, followed by the

addition of 10 µL of a $10^{-5}$ mol/L ethanolic solution of either Rhodamine 6G, 4-aminothiophenol or fluorescein. Samples were let to dry and subsequently kept in 100ºC oven for 10 minutes. Raman analysis was performed immediately after.

Raman spectra were collected in 532 and 633 nm excitation wavelengths focusing in regions of pure gold, silver and copper, with laser power, number of accumulations and exposure time adjusted as required. It should be noticed that Au presents inter-band transitions (at ca. 2.5 eV / 500 nm) promoting an increase in optical absorption and thus a diminution in enhancement when excitation sources approach this energy level. It is also known that Ag particles are prone to oxidation, losing part of the enhancement and fluorescence suppression capabilities.

Chemometric analysis was performed in MATLAB 2015a with the Statistics toolbox, spectra were inputted after standardizing pre-processing step (mean centred and unit variance) and interpolation to match the number of datapoints needed; therefore, all samples contained same number of variables. Non-supervised analysis for principal component (PCA) was employed with covariance matrix calculation (singular value decomposition), generating 17 eigenvectors; three first components account for 77 percent of explained variance. Clustering by hierarchy was performed in Origin 2019 and 100% of the data was correctly grouped; every cluster corresponds to one analyte at one specific wavelength and generated one calculated (but not plotted) central coordinate, used to plot a two standard-distance sphere for visual clarity, 89% of the data is comprehended inside this range. Cluster-to-cluster centroid distances (CD) were simply calculated as the three-dimensional Euclidian distance, a larger distance implies a substantial detected difference. Although the squared of Euclidian distance is often used the previous was chosen to be reported.

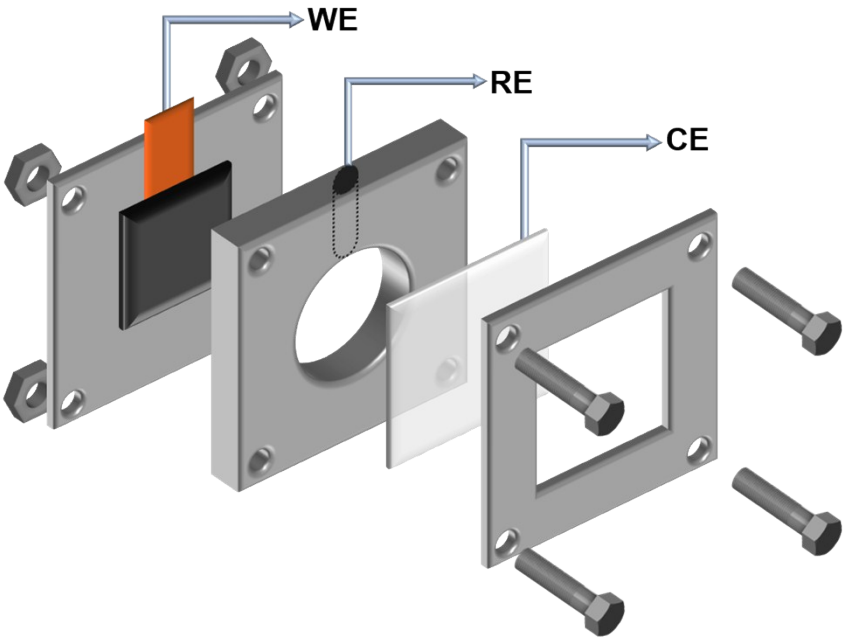


**Figure S2.** Cell configuration used within projector device. A monolayer protected Si piece was attached to copper tape with Ga-In eutectic mixture to ensure electrical contact and fixed to a plastic plate. The middle piece was filled with plating bath and an upper hollow channel connects to a reference electrode. An ITO coated slide was used as both counter electrode and optical window. The cell is tightly

closed with screws and O-rings (not represented) to avoid any leakage. To maximize quality of results: (i) the employed cell (Fig. S2) cannot be disassembled between plating baths exchange as displacements in Si wafer position greatly affect precision of deposition by the next projected image; (ii) a thorough chamber flushing with distilled water is very important so that ions from previous bath are completely removed before refilling with next bath. Often this process creates internal pressure and Si substrate can drift slightly; (iii) ITO employed as counter-electrode is pressed against an O-ring. Care must be taken to avoid excessive curving of the ITO surface that contributes to radial distortion; (iv) cell must be aligned with projected plane as perfectly as possible because small deviations caused by potentiostat connectors can lead to angular distortion of projected image.

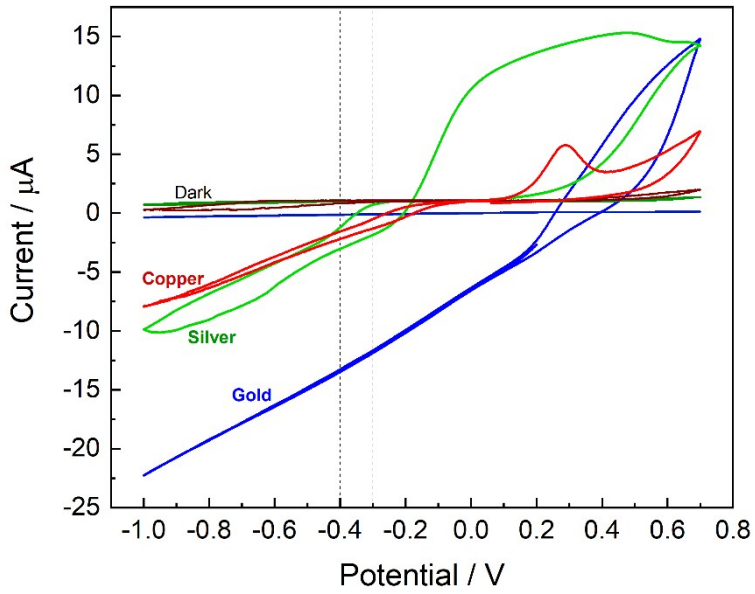


**Figure S3.** Cyclic voltammograms of amorphous silicon in plating baths. Potentials used for deposition of Au and Ag (-0.3 V) are highlighted, as well as the potential used for Cu deposition (-0.4 V). Ag/AgCl/$Cl^-_{3M}$ and Ag-wire were used as reference for deposition of three metals as described in Experimental Section.

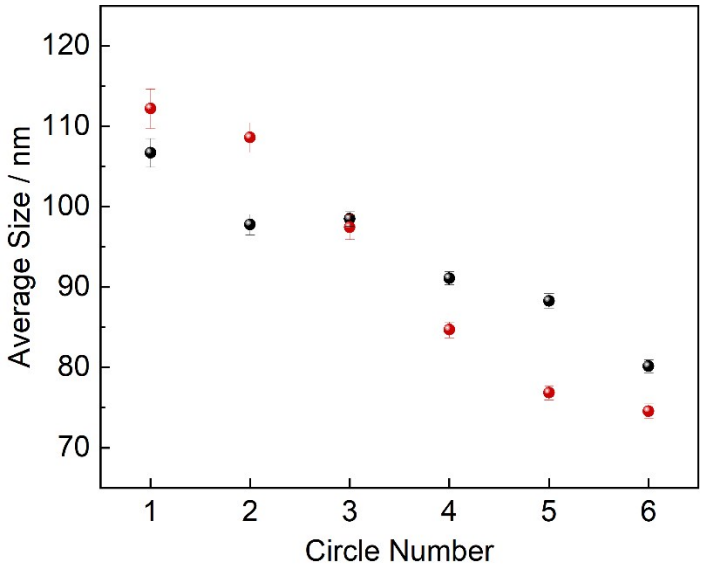


**Figure S4.** Average copper nanoparticle diameter found in each circle after six successive electrodeposition steps onto crystalline (red) and amorphous (black) silicon. $E_{dep}$ = -0.7 V vs $Ag/AgCl/Cl^-_{3M}$ and Q = 75 mC/cm². It must be noticed that in c-Si circle diameter increases, so that area becomes larger each step (up to 50% when comparing first and sixth circle).

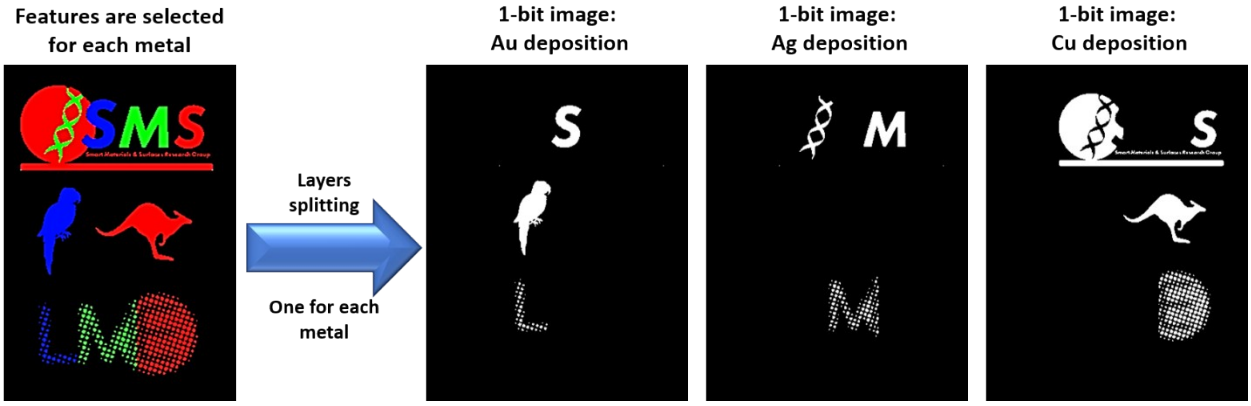


**Figure S5.** Scheme of figures used for the complex image deposition. An image was drawn with all features intended to be transferred to the amorphous silicon surface. The number of metals dictated the minimal number of layers needed, in this case three. One layer for each metal was generated with only the features that should be consisted of that particular metal. The set of three binary layers was loaded to the projector and the spatial data of each pixel (white = 1 = ON and black = 0 = OFF) drove the state of the FLCoS micromirror array, projecting the image onto the amorphous silicon surface.

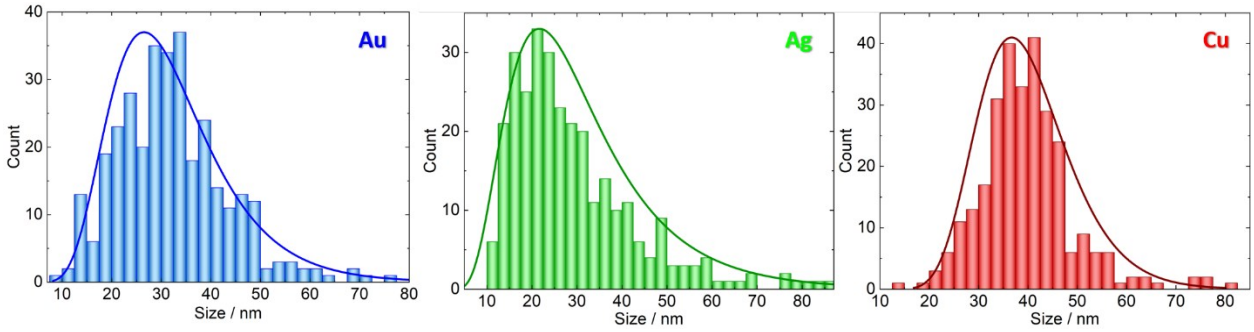


**Figure S6.** Particle diameter distribution for Au, Ag and Cu electrodeposits with log-normal curve added for visual clarity purpose. Average particle sizes of 30 ± 1 nm, 28 ± 2 nm and 39 ± 1 nm respectively. Particles were deposited with potentials of -0.3 V (vs Ag/AgCl/$Cl^-_{3M}$ ), -0.3 V (vs Ag wire) and -0.4 V (vs Ag/AgCl/$Cl^-_{3M}$ ) respectively.

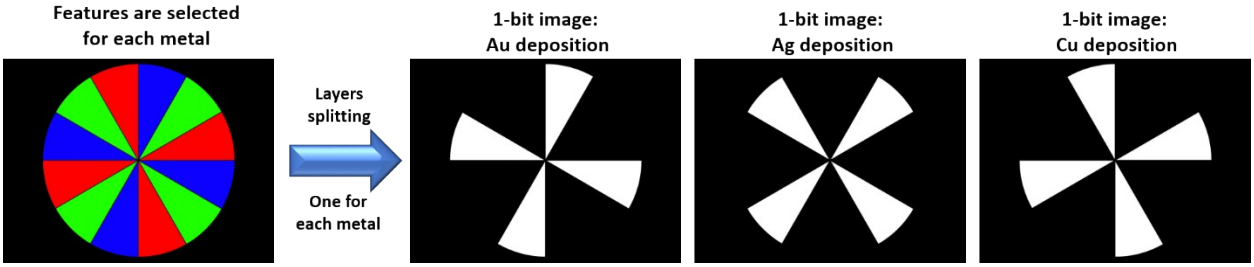


**Figure S7.** Representative scheme of the sectored circle before and after layer-splitting for the three-metallic deposition process. Each metal was deposited in four sectors at the same time. White regions representing 1 valued bits (ON), black regions representing 0 valued bits (OFF).

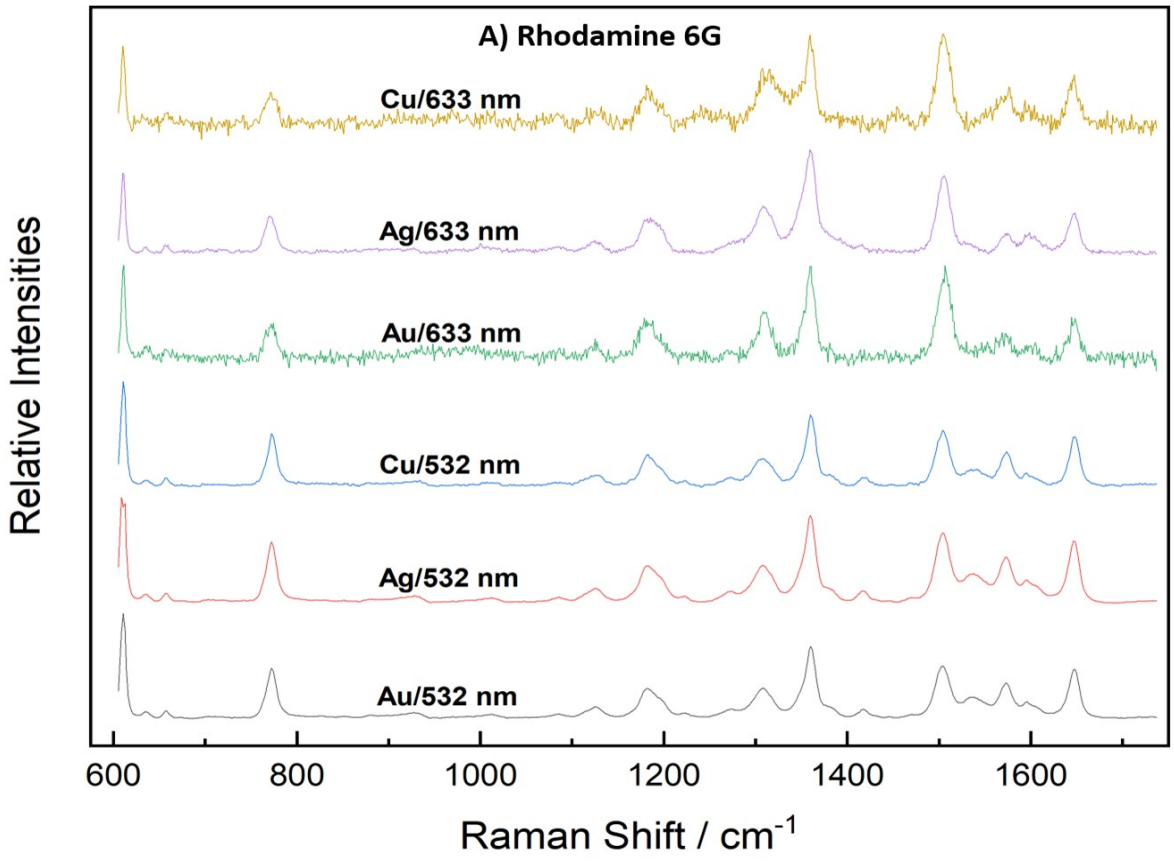
A) Rhodamine 6G
Cu/633 nm
Ag/633 nm
Au/633 nm
Cu/532 nm
Ag/532 nm
Au/532 nm
Relative Intensities
600
800
1000
1200
1400
1600
Raman Shift / cm-1

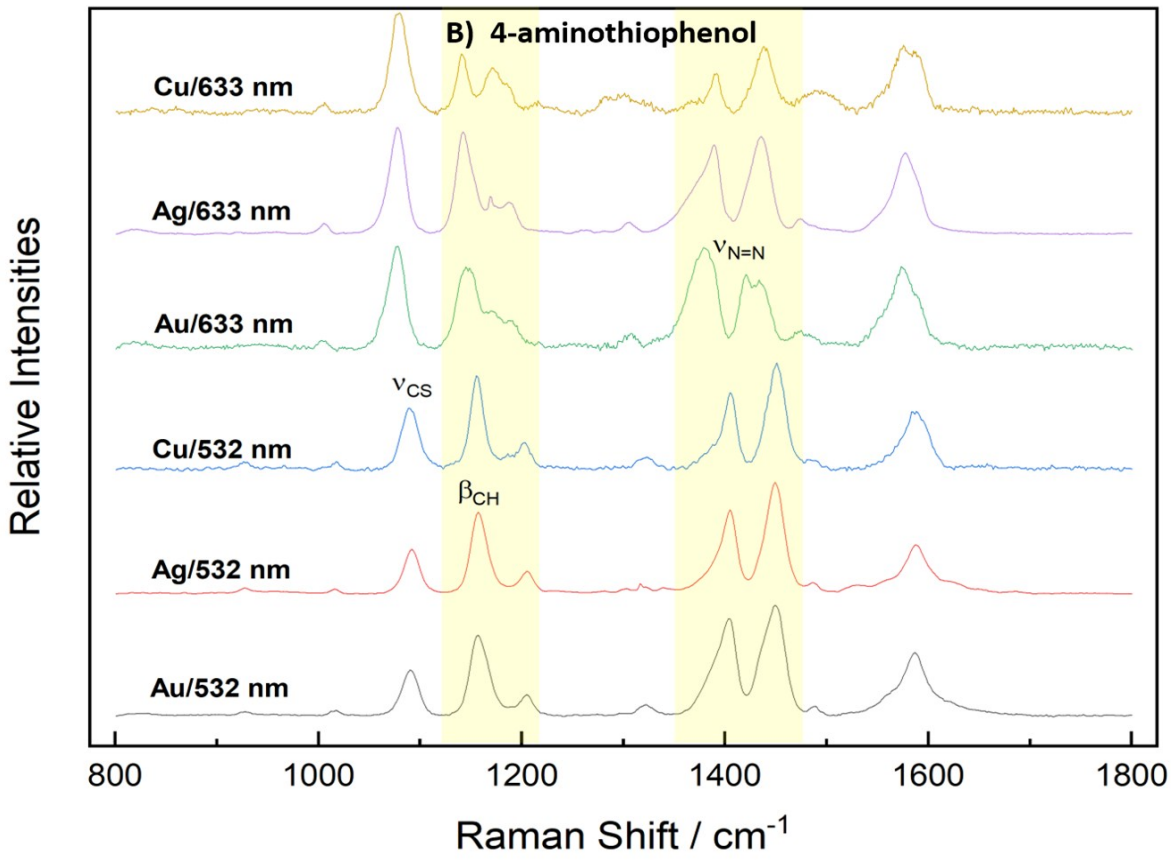
B) 4-aminothiophenol
Cu/633 nm
Ag/633 nm
Au/633 nm
Cu/532 nm
Ag/532 nm
Au/532 nm
$\nu_{N=N}$
$\nu_{CS}$
$\beta_{CH}$
Relative Intensities
800
1000
1200
1400
1600
1800
Raman Shift / cm$^{-1}$

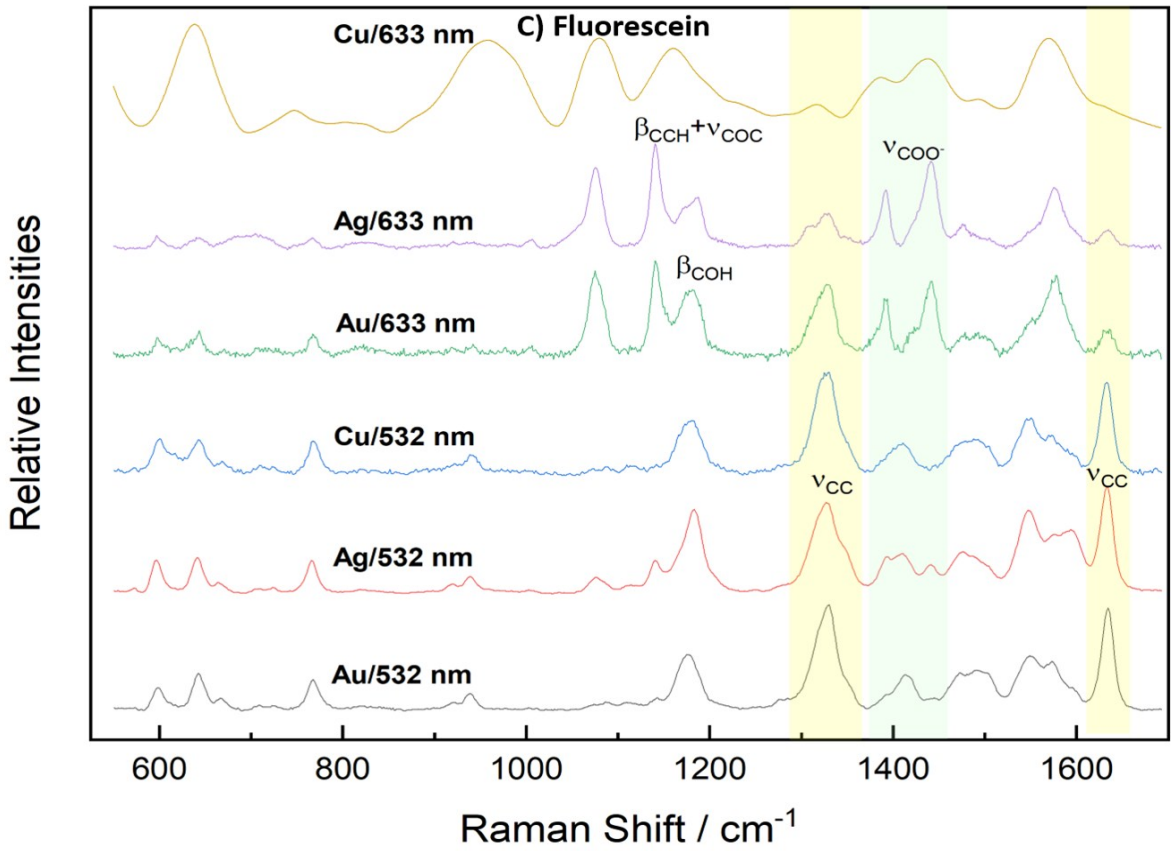


**Figure S8**. Raman spectra of (A) rhodamine 6G, (B) 4-aminothiophenol and (C) fluorescein collected onto Au, Ag and Cu deposits of sectored circle trimetallic platform (as in Fig S6); wavelengths of 532 nm and 633 nm were used. All spectra are standardized, baseline removed and stacked for easiness of comparison. Some vibrational modes are represented either by identification or colour shadowing and are further discussed in main paper. Spectrum "Cu/633 nm" of fluorescein was very weak and noisy, thus an FFT-smoothed version is shown.

1 M. H. Choudhury, S. Ciampi, Y. Yang, R. Tavallaie, Y. Zhu, L. Zarei, V. R. Gonçales and J. J. Gooding, *Chem. Sci.*, 2015, **6**, 6769–6776.